Science Advances
AAAS

advances.sciencemag.org/cgi/content/full/6/49/eabb7242/DC1

Supplementary Materials for

The chaperonin CCT controls T cell receptor–driven 3D configuration of centrioles

N. B. Martin-Cofreces*, F. J. Chichon, E. Calvo, D. Torralba, E. Bustos-Moran, S. G. Dosil, A. Rojas-Gomez, E. Bonzon-Kulichenko, J. A. Lopez, J. Otón, A. Sorrentino, J. C. Zabala, I. Vernos, J. Vazquez, J. M. Valpuesta*, F. Sanchez-Madrid*

*Corresponding author. Email: fsmadrid@salud.madrid.org (F.S.-M.); jmv@cnb.csic.es (J.M.V.); noa.martin@salud.madrid.org (N.B.M.-C.)

Published 2 December 2020, *Sci. Adv.* **6**, eabb7242 (2020)
DOI: 10.1126/sciadv.abb7242

The PDF file includes:

Other Supplementary Material for this manuscript includes the following:

(available at advances.sciencemag.org/cgi/content/full/6/49/eabb7242/DC1)

Supplementary Figure 1

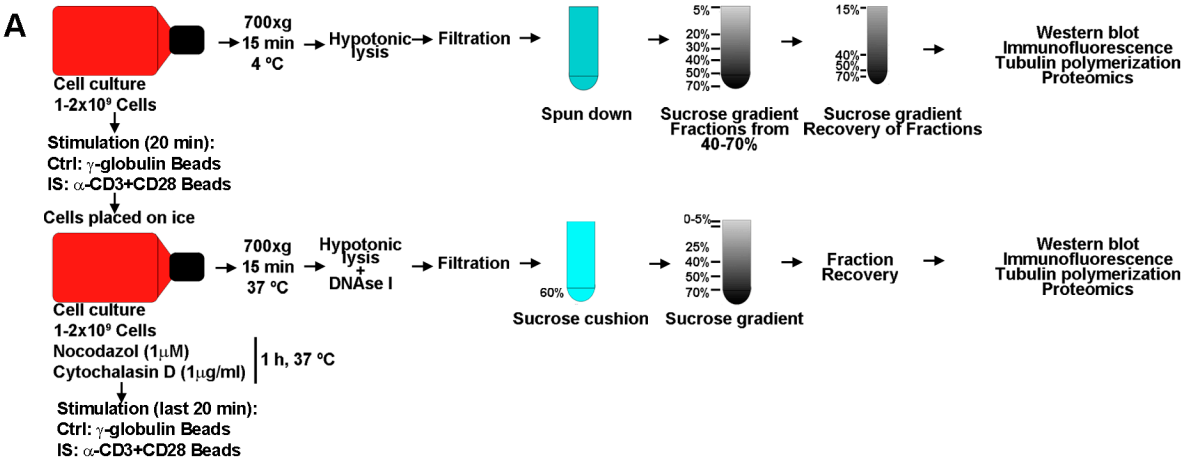

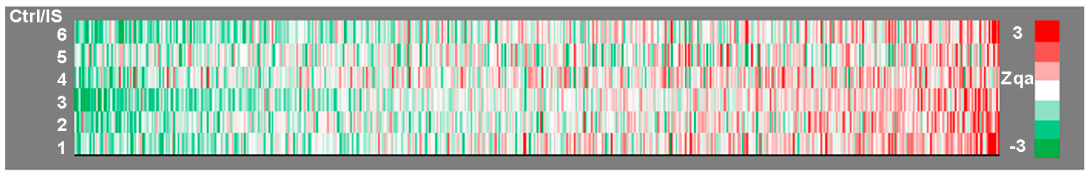

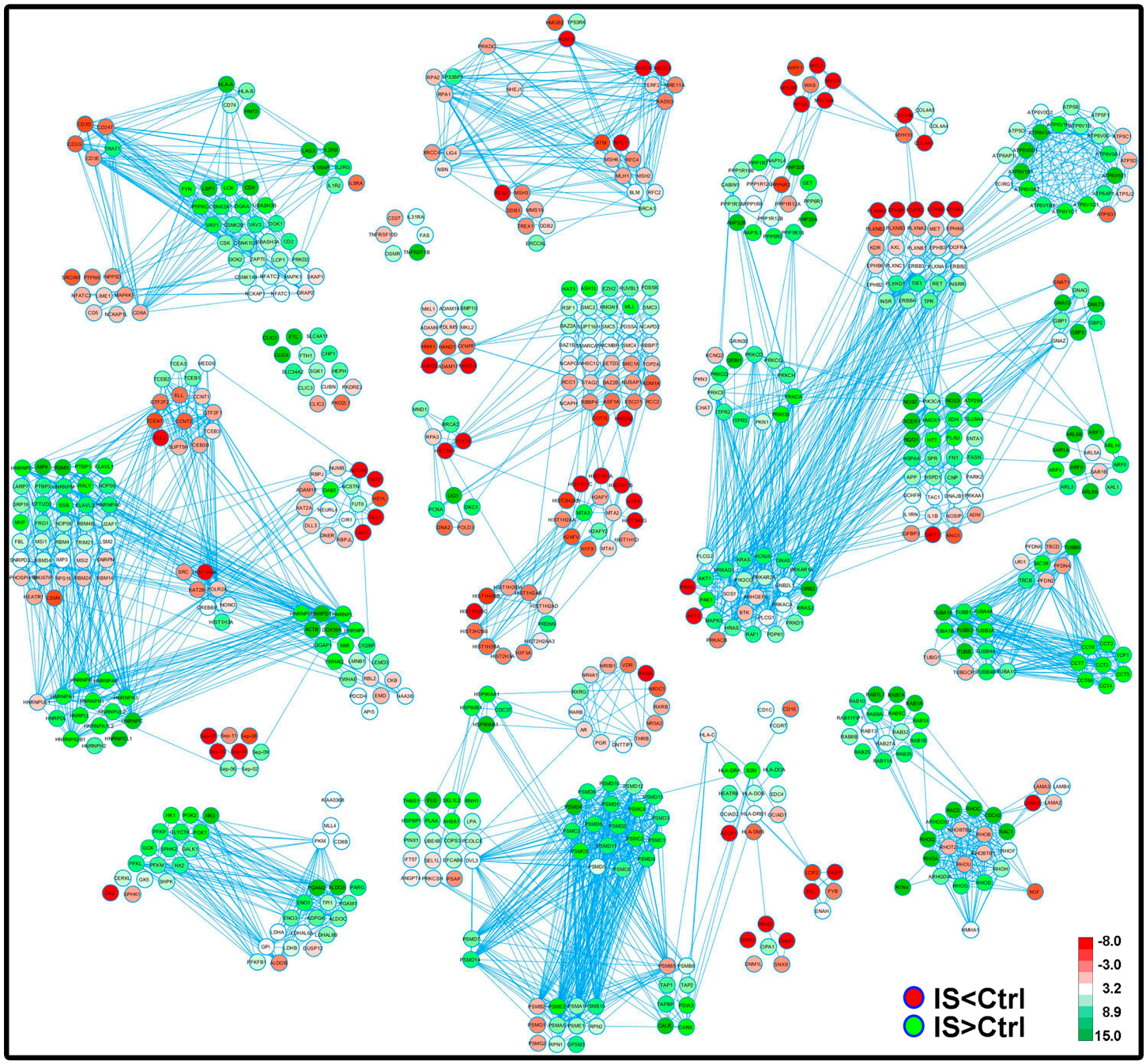

Figure S1. Subcellular fractionation and Systems Biology of centrosome-enriched fractions from human primary T lymphocytes upon polarized T cell Receptor and CD28 activation. (**A**) Scheme depicting procedures for centrosomal isolation in human primary IL-2 expanded T cells (upper panel) and Jurkat T lymphoblastoid cells (lower panel). (**B**) Systems Biology analysis of the 6 biological replicates showing increased (green) and decreased (red) proteins. (C) Complete Cytoscape network for interactions from iTRAQ analysis of centrosome-enriched fractions from human primary T lymphocytes upon polarized T cell Receptor and CD28 activation showing map of interactomes of the stimulated versus resting centrosomes in T cells upon proteomics analysis. **Refers to Fig 1**.

Supplementary Figure 2

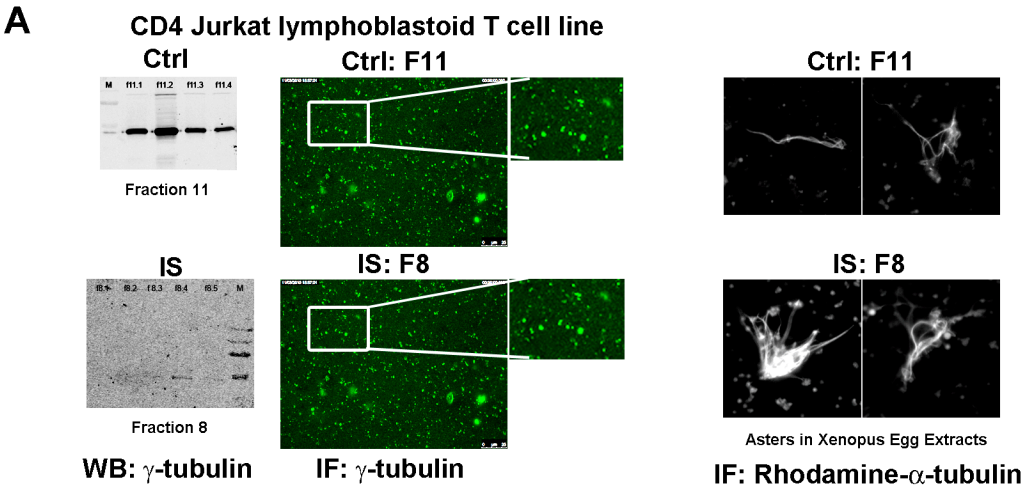

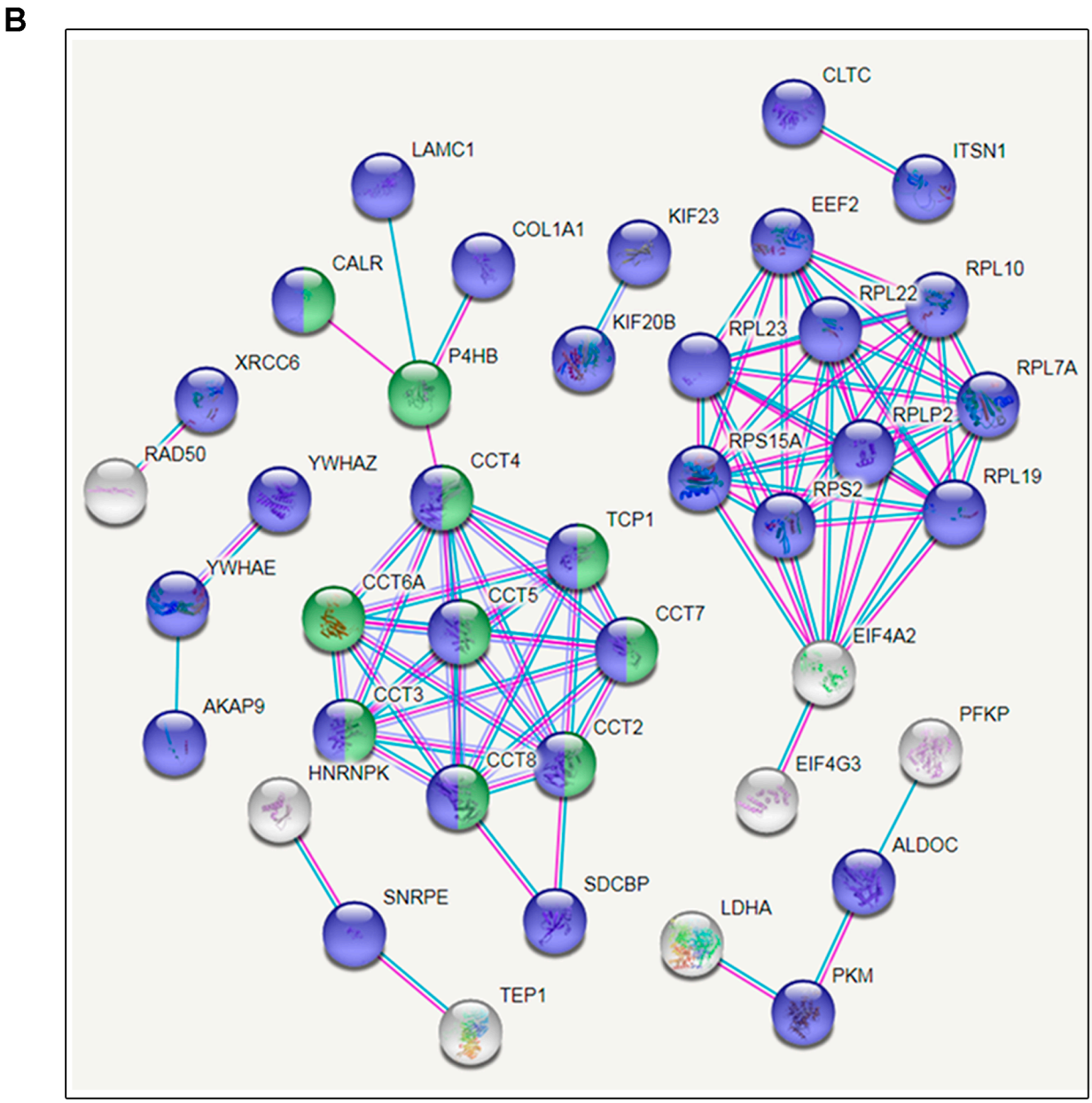

Figure S2. Centrosome-enriched fractions from Jurkat T cells upon TCR and CD28 polarized stimulation. (**A**) Western blot (WB, left panel) and immunofluorescence (IF,a central panel) to assess γ-tubulin content in fractions from a centrosomal isolation procedure for Jurkat lymphoblastoid cells. Selected fractions were used for tubulin polymerization assays in *Xenopus laevis* egg extracts (right panel). (**B**) Results from label-free proteomics experiments from enriched fractions in centrosomes from (**A**) The filtered proteins from data in Table S3 were subjected to interaction network analysis and to category enrichment analysis using STRING (https://string-db.org). Two main categories were obtained including CCT (green) and cellular localization (blue). To construct the network, only the highest confidence (0.900) protein nodes were selected, and the disconnected nodes in the network were hidden. **Refers to Fig 1.**

Supplementary Figure 3

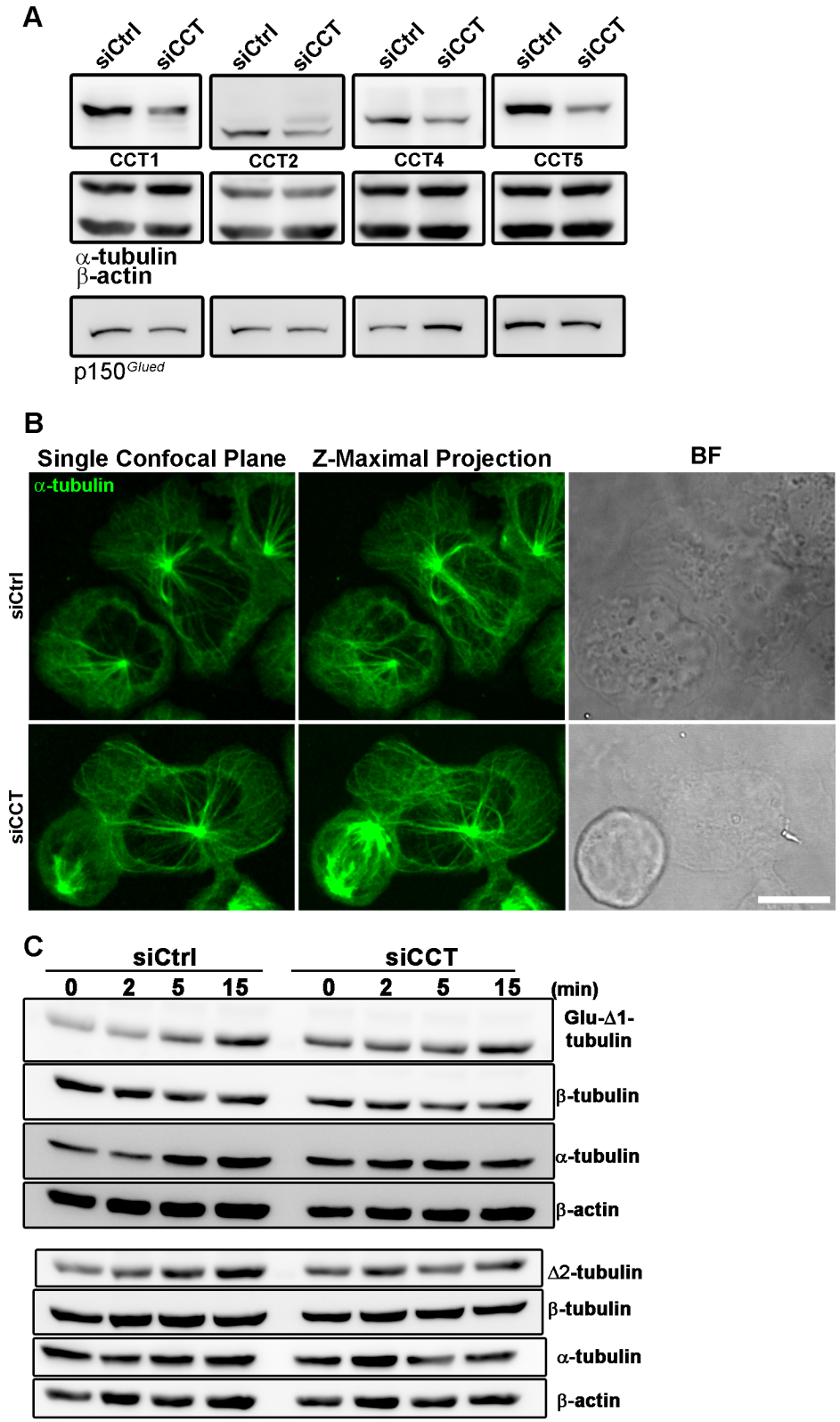

Figure S3. Analysis of tubulin post-translational modifications. (**A**) Jurkat cells were transfected with control or siRNA specific for CCT (siCtrl or siCCT, respectively) and cell lysates were subjected to western blot. α-tubulin and β-actin levels were detected with specific antibodies; p150-glued subunit of dynactin molecular motor complex was used as a loading control in the same membrane. (**B**) Jurkat cells were transfected with control or siRNA specific for CCT (siCtrl or siCCT, respectively) and plated onto poly-L-Lys-coated coverslips, fixed and stained for α-tubulin (green; FITC-conjugated monoclonal antibody DM1A clone). A single confocal slice from the cell base near the substratum and a maximal projection of the Z-stack are shown. BF, bright-field images. Scale Bar = 10 μm. (**C**) Analysis of post-translational modifications in total extracts of cells from A, after activation with anti-CD3ε and anti-CD28 coated-beads for the indicated time, lysed and processed for SDS-PAGE and western blot. **Refers to Fig. 2.**

Supplementary Figure 4

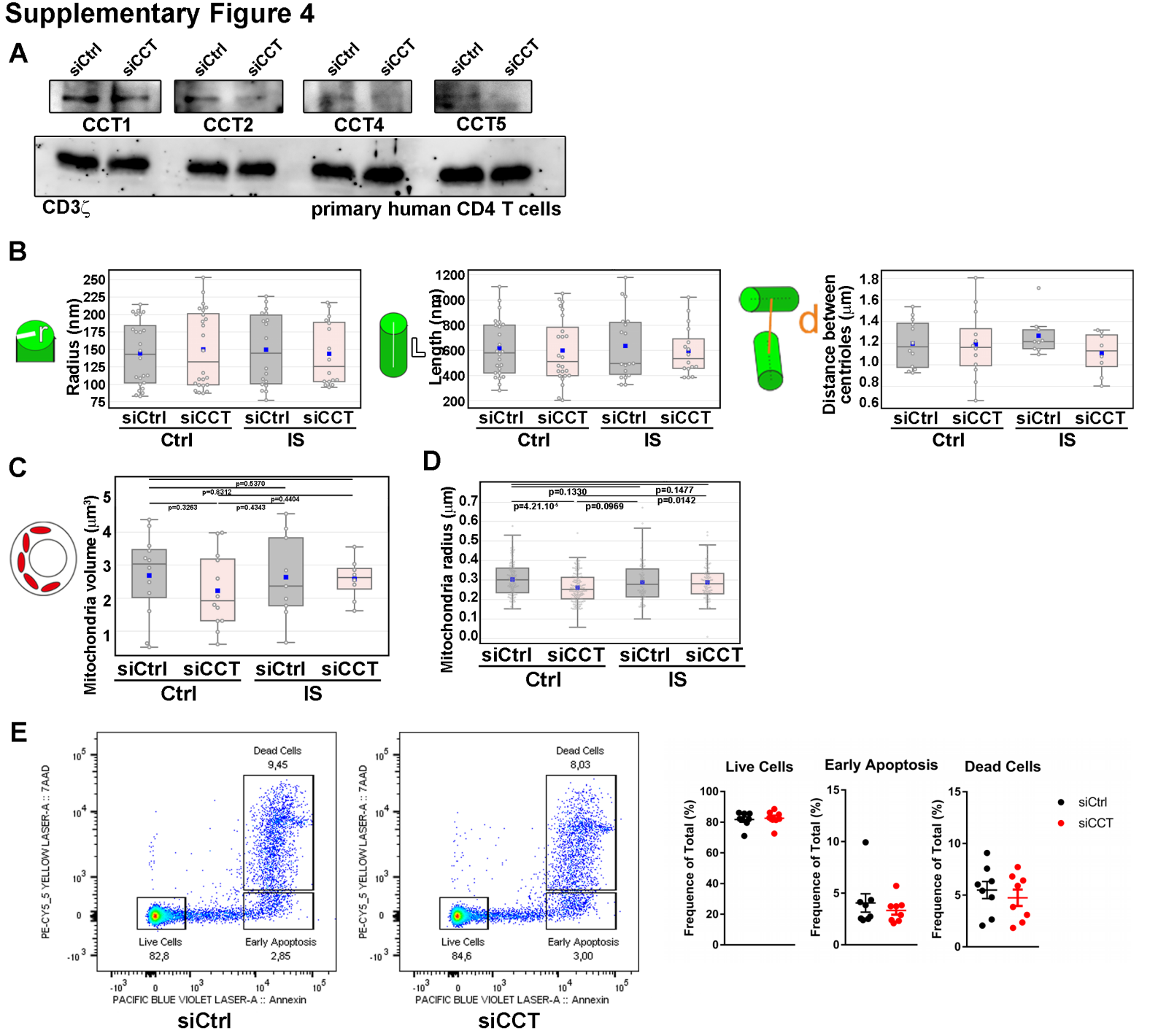

Figure S4. Cryo-Soft-X-Ray imaging of CD4 T cells during IS formation. (A) CCT knock-down in primary CD4 T cells isolated from buffy coats and co-transfected with EB3-GFP and siCCT or siCtrl siRNAs. Cells were sorted for GFP at 48 h post-transfection and used for vitrification and imaging under cryoSXT. CD3ζ was used as loading control in the same membrane. **(B)** Graphs showing estimations of the centriolar radius (r), and the centriolar length (L; n=24, control siCtrl; 24, control siCCT; 18 IS siCtrl and 16 IS siCCT) and the distance between centrioles (d) (corresponds to the modulus or vector magnitude of the vector joining the center of mass of each centriole; n=12, 12, 9 and 8). (**C-D**) Graphs showing estimations of the mitochondria volume per cell (C) and the mitochondria individual radius. (D) (n=12, control siCtrl; 12, control siCCT; 9 IS siCtrl and 8 IS siCCT for mitochondria volume and n=125, control siCtrl; n=158, control siCCT; n=79 IS siCtrl; n=103, IS siCCT). Kruskal-wallis test. (**E**) Apoptosis assay by flow cytometry in resting human CD4 cells knocked-down for CCT; Annexin V and 7-AAD were used to evaluate apoptosis (phophatidyl-serine at the external leaf of the plasma membrane) and cell death, respectively. Graph show the frequency of events for n=8 different donors. Mann-Whitney Test. **Refers to Figure 3 and 4.**

Supplementary Figure 5

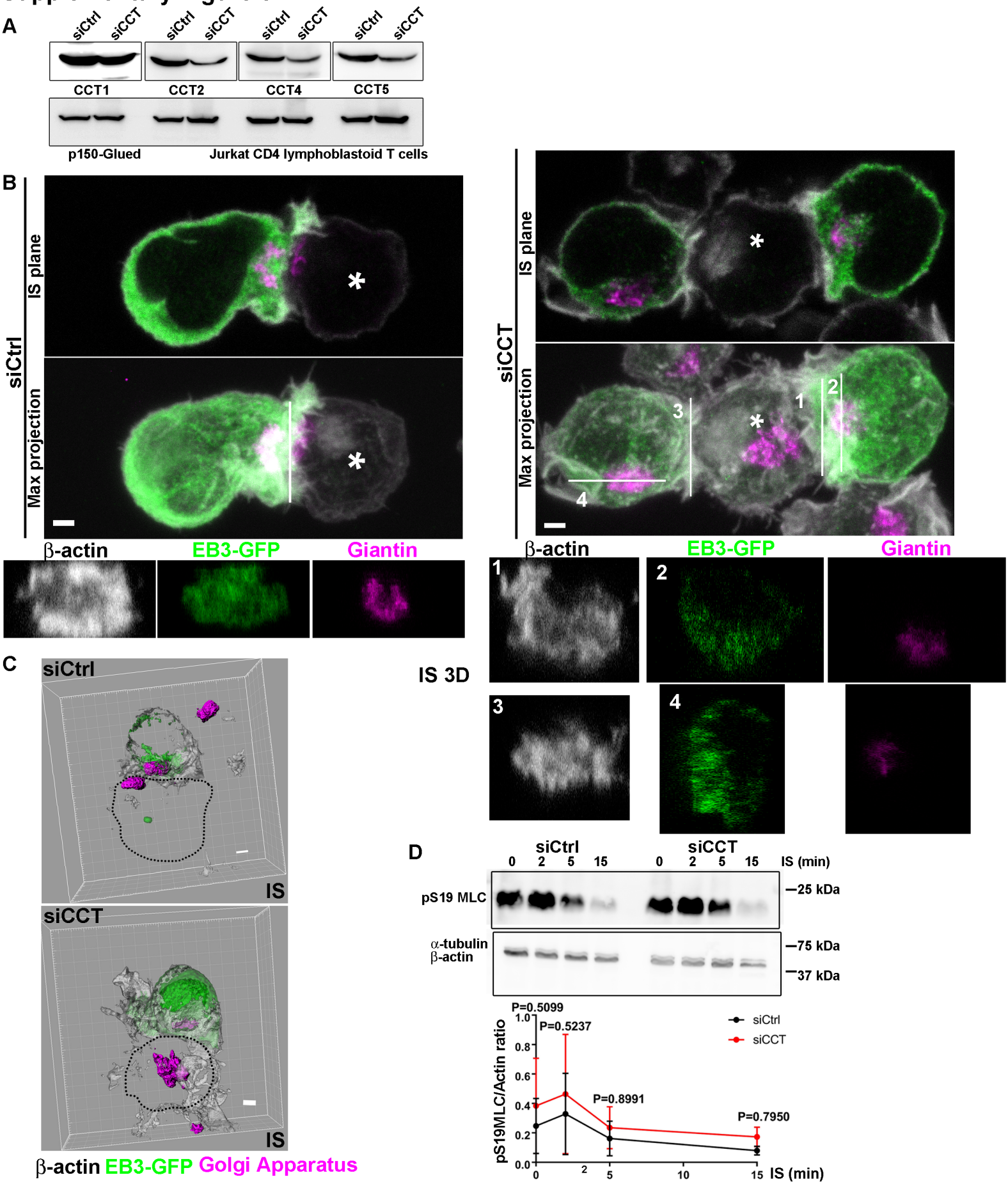

Figure S5. STED imaging of Jurkat T cells during IS formation. (**A**) Jurkat cells were transfected with control or siRNA specific for CCT (siCtrl or siCCT, respectively) and cell lysates were subjected to western blot. p150-glued subunit of the dynactin molecular motor complex was used as loading control in the same membrane. (B) STED fluorescence images of T cells conjugated with SEE-pulsed Raji B cells. T cells were co-transfected with EB3-GFP and siCCT, conjugated to Raji B cells for 30 min, and then cells were fixed and stained for filamentous actin (phalloidin, grey), Golgi apparatus (giantin, magenta) and GFP (green). Images (1-4) correspond to cross-sections described in the upper images generated with Image J. Asterisks correspond to SEE-pulsed Raji B cells (APCs). (C) 3D reconstruction with Imaris software of cell conjugates processed as in (B). Filamentous actin is depicted in grey, Golgi apparatus in magenta and GFP in green. Scale bar = 2 μm. (D) Jurkat cells were transfected with siCCT and stimulated with tetramers (anti-CD3+anti-CD28) for the times indicated. Cell lysates were run on a 15% polyacrylamide SDS-PAGE and subjected to western blot. Phosphorylated myosin light chain (pS19MLC), tubulin and actin were assayed (loading controls). Graph, densitometry ratio (two-way ANOVA, n=4). **Refers to Figure 5**.

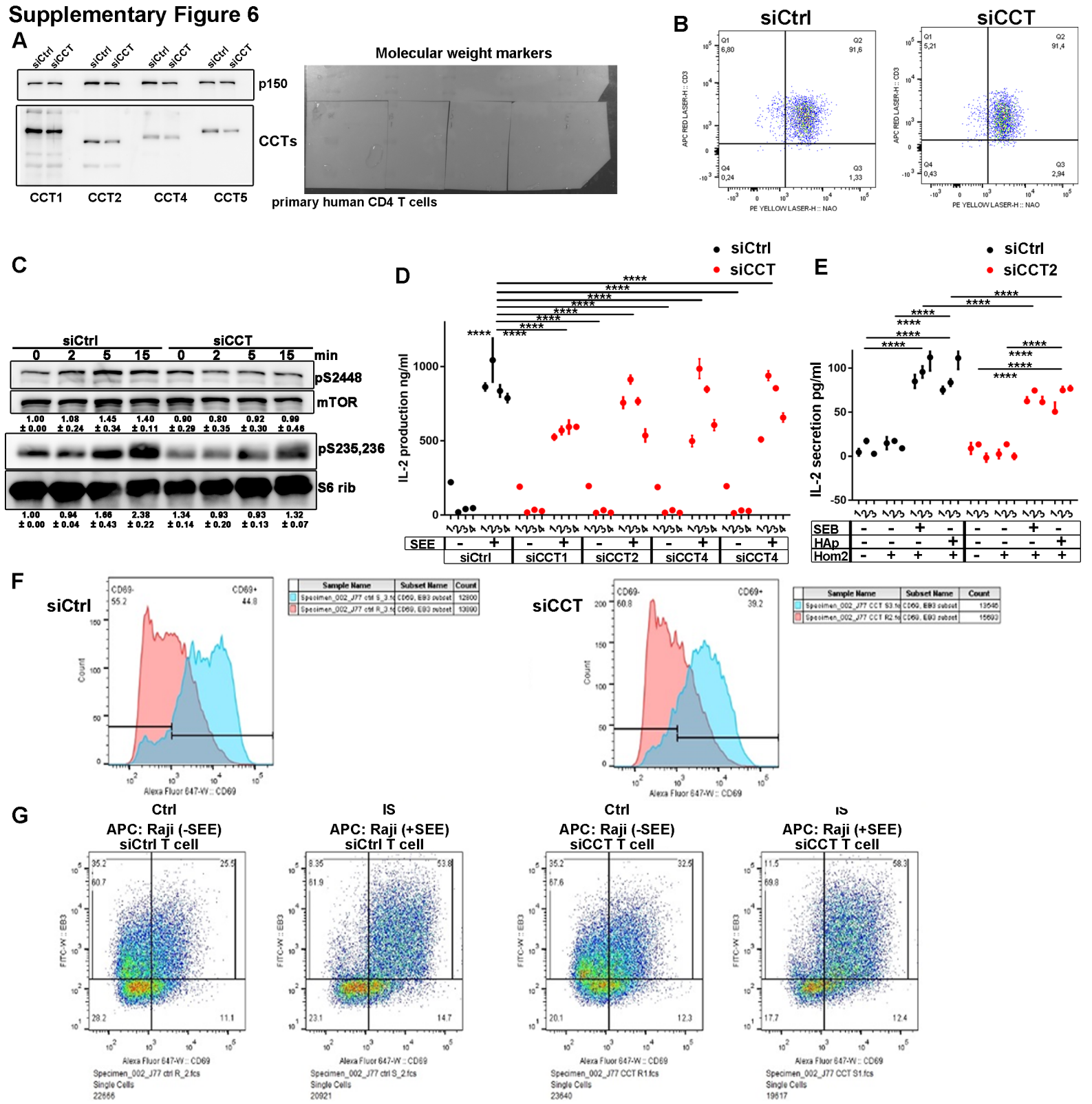

Figure S6. siCCT affects late markers of T cell activation but not early markers: effect on IL-2 secretion and CD69 expression in activated T cells. (**A**) Western blot showing CCT silencing in human primary CD4 T cells. A chemoluminescence image and visible image for molecular weight markers are included. (**B**) Flow Cytometry analysis of mitochondrial mass by Nonyl-acridine Orange (NAO) staining in human CD4 cells. CD3e expression is also shown. (**C**) Metabolic constraint in Jurkat T cells by CCT knock-down during immune synapse. Analysis of mTOR and S6 phosphorylation by western blot is shown; numbers correspond to normalized ratio for fold induction (time 0, siCtrl cells; mean and SD, n=2). (**D**) IL-2 secretion measured by ELISA from supernatant of co-cultured Raji cells (+/- SEE) and Jurkat cells transfected with siRNAs specific for individual CCT subunits (CCT1, CCT2, CCT3 and CCT4). Triplicates of co-cultures were performed for 4 different transfections; two-way ANOVA test with Dunnet's multiple comparison test; ****, p<0.0001. (**E**) CH7C17 Jurkat cells were transfected with siRNA specific for CCT2 and activated with specific HA peptide or SEB superantigen. Triplicates of co-cultures were performed for 3 different transfections; two-way ANOVA test with Tukey's multiple comparison test; ****, p<0.0001. (**F**) Flow cytometry analysis of CD69 expression in T cells conjugated for 18 h with Raji B cells, pulsed or not with SEB. T cells were cotransfected with EB3-GFP and siCCT, and sorted by GFP at 48 h post-transfection. T cells and Raji B cells were co-cultured overnight and stained for CD69. Dead cells were excluded from the analysis. Red, resting T cells; blue, T cells forming an IS. (**G**) Dot blots for gating strategy, showing co-cultures of T and B cells, analyzed in A. EB3-GFP and anti-human CD69 plus anti Alexa 647-conjugated anti-mouse antibody are shown. The spectrum color scale indicates cell number. **Refers to Fig. 5 and 6.**

Table S1.

List of quantified proteins in centrosomes from activated human T cells. Table S1 is provided as an .xlsx file.

Table S2.

List of functional protein categories significantly altered by T-cell activation as a consequence of a coordinated protein response in human centrosomes (FDR<5%). Table S2 is provided as an .xlsx file.

Table S3.

List of identified proteins in label-free experiments from Jurkat centrosomes. The protein list was filtered according to two parameters: proteins present only in activated cells sample (and absent in the controls), and identified with at least 2 different peptides. One protein (CCT7) was manually added to the list since it belongs to the CCT category, even though this protein was identified with two peptides in the control sample. Some centromere proteins were also included on the list to assess the specificity of the analyzed fractions in each case. STRING analysis (https://string-db.org) was performed with the filtered protein list (see Fig. S3B). Table S3 is provided as an .xlsx file.

Movie S1.

Tracking of EB3-GFP-decorated plus-end tips of microtubules at the immune synapse. Jurkat T cells expressing EB3-GFP and treated with control or siRNAs specific for CCT were allowed to settle on stimulatory anti-CD3ε+anti-CD28 coated surfaces and recorded by TIRFm upon excitation with a 488-nm laser at 150 nm of penetrance. Images were taken every 300 ms.

Movie S2.

Visualization of MAP7-GFP decorated microtubules at the immune synapse. Jurkat T cells expressing MAP7-GFP and treated with control or CCT-specific siRNAs were allowed to settle on stimulatory anti-CD3ε+anti-CD28 -coated surfaces and recorded by TIRFm upon excitation with a 488-nm laser at 150 nm of penetrance. Images were taken every 5 s.

Movie S3.

Tracking of EB3-RFP decorated plus-end tips of microtubules upon inhibition of protein synthesis at the immune synapse. Jurkat T cells expressing EB3-RFP and treated or not with cycloheximide were allowed to settle on stimulatory anti-CD3ε+anti-CD28-coated surfaces and recorded by TIRFm upon excitation with a 561-nm laser at 150 nm of penetrance. Images were taken every 300 ms. Imaris Software was used to recognize the fluorescence and to calculate the trajectories, their duration and growing speed.

Movie S4.

Tracking of EB3-GFP decorated plus-end tips of microtubules upon inhibition of proteasome activity at the immune synapse. Jurkat T cells stably expressing low levels of EB3-GFP and treated or not with bortezomib were allowed to settle on stimulatory anti-CD3ε+anti-CD28-coated surfaces and recorded by TIRFm upon excitation with a 488-nm laser at 150 nm of penetrance. Images were taken every 300 ms. Imaris Software was used to recognize the fluorescence and to calculate the trajectories, their duration and growing speed.

Movie S5.

3D reconstruction of non-stimulated control CD4 T cells at nanometric resolution. 3D reconstructions of cryosoft X-ray tomography images from the ALBA synchrotron (Barcelona) showing resting human primary CD4 T cells from healthy donors after treatment with control siRNAs. Cells were allowed to spread onto control grids, vitrified and maintained in liquid nitrogen. The nucleus is segmented in blue and the plasma membrane as a transparent grid. Mitochondria are shown in red, centrioles in green, vesicles in white and lipid droplets in yellow.

Movie S6.

3D reconstruction of non-stimulated siCCT-treated CD4 T cells at nanometric resolution. 3D reconstructions of cryosoft X-ray tomography images from the ALBA synchrotron (Barcelona) showing resting human primary CD4 T cells from healthy donors after treatment with siRNAs specific for CCT. Cells were allowed to spread onto control grids, vitrified and maintained in liquid nitrogen. The nucleus is segmented in blue and the plasma membrane as a transparent grid. Mitochondria are shown in red, centrioles in green, vesicles in white and lipid droplets in yellow.

Movie S7.

3D reconstruction of control CD4 T cells forming an immune synapse at nanometric resolution. 3D reconstructions of cryosoft X-ray tomography images from the ALBA synchrotron (Barcelona) showing human primary CD4 T cells from healthy donors after treatment with control siRNAs. Cells were allowed to spread onto stimulating anti-CD3ε and anti-CD28-coated grids, vitrified and maintained in liquid nitrogen. The nucleus is segmented in blue and the plasma membrane as a transparent grid. Mitochondria are shown in red, centrioles in green, vesicles in white and lipid droplets in yellow.

Movie S8.

3D reconstruction of siCCT-treated CD4 T cells forming an immune synapse at nanometric resolution. 3D reconstructions of cryoSXT images from the ALBA synchrotron (Barcelona) showing human primary CD4 T cells from healthy donors after treatment with siRNAs specific for CCT. Cells were allowed to spread onto stimulating anti-CD3ε and anti-CD28-coated grids, vitrified and maintained in liquid nitrogen. The nucleus is segmented in blue and the plasma membrane as a transparent grid. Mitochondria are shown in red, centrioles in green, vesicles in white and lipid droplets in yellow.

Movie S9.

Imaging of EB3-GFP decorated microtubules in control T cells during immune synapse formation. Jurkat T cells expressing EB3-GFP were allowed to settle on stimulatory anti-CD3ε+anti-CD28-coated surfaces and recorded by resonant scanner confocal at 8000 Hz. Z-stacks were taken by confocal microscopy every 1 s.

Movie S10.

Tracking of CD3ζ-bearing vesicles at the immune synapse. Jurkat T cells expressing CD3ζ-mCherry and treated with control or CCT-specific siRNAs were allowed to settle on stimulatory anti-CD3ε+anti-CD28-coated surfaces and recorded by TIRFm upon excitation with a 561-nm laser at 200 nm of penetrance. Images were taken every 100 ms.

Movie S11.

Imaging of MAP7-GFP decorated microtubules and mitochondria in control T cells at the immune synapse. Jurkat T cells expressing MAP7-GFP and treated with control siRNAs were labeled with MitoTracker Orange, allowed to settle on stimulatory anti-CD3ε+anti-CD28-coated surfaces and recorded by TIRFm upon excitation with 488-nm and 561-nm lasers at 200 nm of penetrance. Images were taken every 2 s. Bright and contrast were adjusted for better visualization with Fiji (Image J) Software.

Movie S12.

Imaging of MAP7-GFP decorated microtubules and mitochondria in CCT-silenced T cells at the immune synapse. Jurkat T cells expressing MAP7-GFP and treated with siRNAs specific for CCT were labeled with MitoTracker Orange, allowed to settle on stimulatory anti-CD3ε+anti-CD28-coated surfaces and recorded by TIRFm upon excitation with 488-nm and 561-nm lasers at 200 nm of penetrance. Images were taken every 2 s. Bright and contrast were adjusted for better visualization of details with Fiji (Image J) Software.

Movie S13.

3D reconstruction of mitochondria from control T cells forming an immune synapse . Jurkat T cells expressing EB3-GFP and treated with control siRNAs were labeled with MitoTracker Orange, allowed to settle on stimulatory anti-CD3ε+anti-CD28-coated surfaces and fixed after 45 min of activation. Cells were imaged by STED microscopy, and 3D reconstructions were performed with LEICA accompanying software.

Movie S14.

3D reconstruction of mitochondria from siCCT-treated T cells forming an immune synapse. Jurkat T cells expressing EB3-GFP and treated with siRNAs specific for CCT were labeled with MitoTracker Orange, allowed to settle on stimulatory anti-CD3ε+anti-CD28-coated surfaces and fixed after 45 min of activation. Cells were imaged by STED microscopy, and 3D reconstructions were performed with LEICA accompanying software.

Movie S15.

Tracking of mean fluorescence intensity of mitochondria at the immune synapse in control and siCCT-treated T cells T cells. Analysis with Fiji (Image J) Software showing the progress of mean fluorescence intensity corresponding to control or CCT-silenced Jurkat T cells labeled with MitoTracker Orange over time, allowed to settle on stimulatory anti-CD3ε+anti-CD28-coated surfaces and recorded by TIRFm.

Movie S16.

Imaging of EB3-GFP decorated microtubules and mitochondria in control T cells during conjugate formation. Jurkat T cells were co-transfected with EB3-GFP and control siRNA, labeled with MitoTracker Orange, and allowed to conjugate with SEE-pulsed Raji B cells (APC; blue: DAPI). Z-stacks were taken by confocal microscopy every 30 s.

Movie S17.

Imaging of EB3-GFP decorated microtubules and mitochondria in siCCT-treated T cells during conjugate formation. Jurkat T cells were co-transfected with EB3-GFP and siRNA specific for CCT, labeled with MitoTracker Orange, and allowed to conjugate with SEE-pulsed Raji B cells (APC; blue: DAPI). Z-stacks were taken by confocal microscopy every 30 s.

Linear Mixed Model.

Linear Mixed Model statistic analysis of mitochondrial respiration (OCR and ECAR data) from Seahorse experiments (Mitostress Test).